Phase dependence and mechanical and thermal ductility of the luminescence properties of tetranuclear Cu(i) metallacycle assemblies stabilized by ditopic organo-pnictogen (P,As) ligands

Constance Lecourt, Raquel Utrera Melero, Jana Schiller, Florent Moutier, Vincent Dorcet, Guillaume Calvez, Corentin Poidevin, Karine Costuas, Manfred Scheer, Christophe Lescop

Phase dependence and mechano and thermal ductility of the luminescence properties of tetranuclear Cu(I) metallacycle assemblies stabilized by ditopic organo-pnictogen (P, As) ligands.

Constance Lecourt,[a] Raquel Utrera Melero,[a] Jana Schiller,[a,b] Florent Moutier,[a] Vincent Dorcet,[a] Guillaume Calvez,[a] Corentin Poidevin,[a] Karine Costuas,*[a] Manfred Scheer*[b] and Christophe Lescop*[a]

Introduction

An ever-rising attention is devoted to the study of luminescent Cu(I)–based derivatives as new photo-functional molecular materials for emitting devices or/and luminescent sensors. Such derivatives offer particularly appealing perspectives for future developments, not only due of the relatively high abundance and low cost of copper offering a competitive alternative to the well-known phosphorescent compounds based on expensive heavy metal complexes, but also regarding the various photophysical properties these Cu(I) complexes exhibit.[1–46] Indeed, emission covering the full visible light spectrum have been reported for such compounds, combined with a large diversity of radiative relaxation processes, including very efficient Thermally Activated Delayed Fluorescence (TADF) processes.[7,8,13–36] In such complexes presenting TADF properties, spatially well-separated HOMO and LUMO orbitals induce small energy gap between the lowest energy singlet-triplet states. This enables a thermal population of the lowest energy excited singlet state (S_1) from the lowest energy triplet excited state (T_1), *via* a reverse intersystem crossing (RISC). Consequently, efficient radiative relaxation processes from this thermally populated S_1 state to the ground state S_0 can take place allowing exalted solid-state luminescence properties

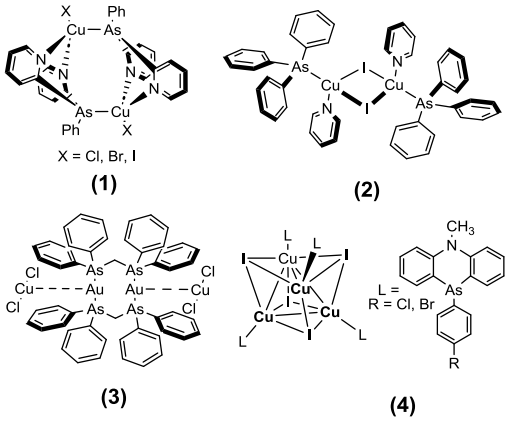

Scheme 1 Molecular structure of the derivatives **1**,[49] **2**,[50] **3**[51] and **4**.[52,53]

close to room temperature (RT). Importantly, in Cu(I)-polynuclear systems, non-covalent cuprophilic interactions characterized by short intermetallic distances (d(Cu-Cu) bellow *ca.* 2.9 Å)[47] can be found in the ground state and/or in the excited state relaxed geometries.[32,33] Such interactions induce an enhancement of the spin-orbit coupling (SOC) constants compared to the one observed with non-interacting Cu(I) ions for which intrinsic individual SOC is generally moderate. Consequently, the radiative rate constants for the T_1 state are increased, promoting efficient RISC to the S_1 state but also a fast and efficient phosphorescent relaxation process to the ground state (S_0).[48]

In order to prepare emissive Cu(I) assemblies bearing larger SOC constant value and likely improved radiative relaxation rates and luminescence properties, one approach could consist in the introduction of heavy donor elements bearing high individual SOC values in the coordination sphere of the Cu(I) ions. Interestingly, a general synthetic strategy toward highly luminescent Cu(I)–based systems relies on the use of aromatic organophosphorus ligands that confer a remarkable stability to Cu(I) complexes but also, very frequently, generate electronic configuration promoting emergence of TADF properties. In a marked contrast, the use of analogous heavier pnictogen-based ligands, in particular arsines, remains particularly scarce while such ligands could be advantageous over lighter pnictogen donors due to higher intrinsic SOC (such as $\xi = 1202$ cm^{-1} for As atom while $\xi = 230$ cm^{-1} for P atom).[54] Thus, Artem'ev *et al.* described recently the preparation and the photophysical studies of a series of complexes **1** (Scheme 1) in which CuX (X = Cl, Br, I) sub-units are stabilized by the bis(2-pyridyl)phenylarsine ligand.[49] It was reported that these derivatives present short-lived luminescence at RT assigned to a combination of fast phosphorescence and TADF processes. Interestingly, these dinuclear Cu(I)–arsine complexes displayed significantly shorter decay times than their phosphine analogous, which was tentatively assigned to a consequence of the higher SOC strength carried by the arsenic atoms *versus* phosphorus atoms. in 2020 Naka *et al.* reported the study of 'Cu_2I_2'-based bimetallic phosphorescent complexes **2** (Scheme 1) stabilized by the triphenylarsine ligand and showing mechanochromic luminescence properties.[50] In 2021, this group also reported a comparative study of the effect of a arsenic ligand (bis(diphenylarsino)methane) *versus* its phosphorus-based congener (bis(diphenylphosphino)methane, dppm) on the formation of inter- and intramolecular metallophilic interactions in Au(I)-Cu(I) ionic-pair luminescent derivatives **3** (Scheme 1).[51] In 2021, Karasik *et al.* developed a series of $\{Cu_4I_4L_4\}$ cubane-based clusters **4** (Scheme 1) bearing arsine ligands to study the effect of the presence of the arsenic

heavy atom on the HE (high energy) band emission of the cluster.[52,53]

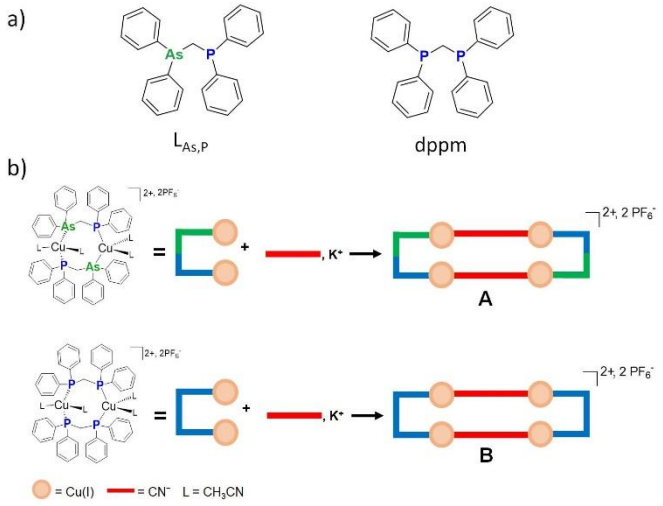

Scheme 2 a) Molecular structure of the ligands $\mathbf{L_{As,P}}$ and dppm, b) Syntheses and schematic description of the tetrametallic metallacycles **A** and **B**.

These studies triggered our interest for exploring such potential impact of the replacement of phosphorus donor atoms by arsenic donor atoms in ligands coordinated to Cu(I) metal centers on the alteration of photophysical properties of the resulting complexes. Herein, we report the preparation of a tetrametallic Cu(I) metallacycle **A** (Scheme 2) stabilized by the ''mixed'' arsenic-phosphorus bridging ligand [(diphenylarsino)methyl]diphenylphosphane $\mathbf{L_{As,P}}$ (Scheme 2a). This tetrametallic assembly is obtained considering an adaptation of the coordination-driven supramolecular synthetic approach. Its synthesis, characterization, X-ray single crystal molecular structure and solid-state luminescence properties are reported and compared to its analogous tetrametallic compound **B** (Schemes 2b) previously published by our group, based on the diphosphine dppm ligand.[32] Density functional theory (DFT) calculations reveal that the SOC of the heavier arsenic element does not show a direct influence on the photophysical properties in **A** compared to the derivative **B**. However, the establishment of structure-property relationships reveals an impact of the $\mathbf{L_{As,P}}$ ligand on the crystalline packing of **A** compared to the organization observed in the crystals of the lighter congener species **B**. This raises the question of the relative impacts of the SOC values on the luminescence efficiencies of these derivatives *versus* the extended supramolecular organizations in the crystalline solid-states. In line with this point, luminescent thermochromism and mechanochromism are observed and analyzed for both **A** and **B** assemblies, that moreover also display in the solid-state at high temperature an original irreversible thermal crystalline transition that impacts their photophysical properties. All in all, this study highlights the subtle and competitive effects that can rule out the photophysics of Cu(I) polymetallic assemblies based on organo-pnictogen ligands and reveals their stimuli-sensitive behaviours, allowing the facile preparation of different phases bearing contrasted efficient luminescence properties.

Results and discussion

Preparation and characterization of the tetrametallic metallacycle A

The high flexibility presented by Cu(I) metal complexes was in general initially considered as being very detrimental in the perspective of designing highly luminescent Cu(I) complexes. Indeed, it allows easy geometrical re-organization processes to be activated in the excited states, connected with fast nonradiative decay rates and concomitant small RT emission quantum yields. Such unfavorable situation was firstly avoided by coordinating Cu(I) ion with bulky chelating ligands.[8] As a result, little freedom for distortions in the exited state is imposed to the Cu(I) ion's coordination sphere and RT photoluminescence quantum yields as high as the unity can be measured in particular in systems where TADF relaxation processes take place. In an alternative approach, in 2016 Yam and Lescop described the selective preparation of the sterically constrained highly emissive tetrametallic Cu(I) metallacycle **B** (Scheme 2b) from the self-assembly reaction of the pre-assembled bimetallic precursor $[Cu_2(\mu_2\text{-dppm})_2]^{2+}$ with cyanide connecting ligands.[32] Within this tetrametallic assembly bearing multiple chelates and metallacycle subunits, the Cu(I) ions' coordination sphere can undergo only reduced structural re-organization alteration in the excited states at the time scale of the photoexcitation events, due to the high energetic cost of such process over the whole constrained polycyclic architecture. Consequently, non-radiative deactivation pathways are disfavored which promotes emergence of enhanced solid-state photophysical properties in these self-assembled derivatives, also likely favored by the cuprophilic interactions observed within this assembly (d(Cu-Cu) = 2.866(9) Å in the $[Cu_2(\mu_2\text{-dppm})_2]^{2+}$ subunits). Indeed, the derivative **B** reveals to be an efficient TADF luminophore, emitting in the solid state at RT upon photoexcitation an eye-perceived blue light with a remarkable emission quantum yield of 72 %.

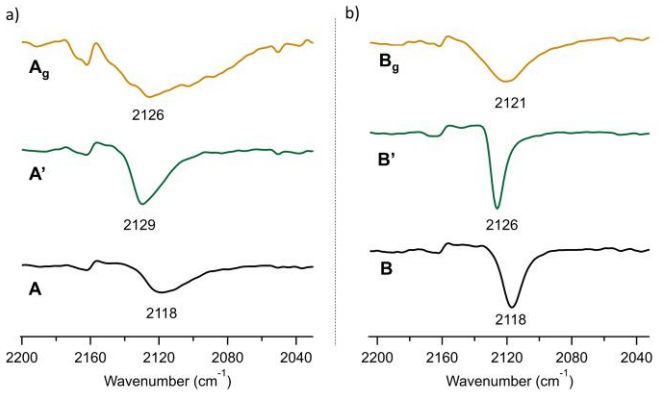

Fig. 1 Infra-red spectra centered on υ(C≡N) vibrational bands of a) derivatives **A**, **A'**, $\mathbf{A_g}$ and b) derivatives **B**, **B'**, $\mathbf{B_g}$.

This result motivated us to replace the chelating dppm ligand by its $\mathbf{L_{As,P}}$ analog ligand and to explore whether similar self-assembling could take upon its combination with Cu(I) metal centers and cyanide ligands. The synthesis of the $\mathbf{L_{As,P}}$ chelating ligand was conducted based on an adaptation of a previously reported procedure,[55,56] heating Ph_2AsCl at its reflux point with Ph_2PCH_2-TMS (TMS: trimethylsilyl) under inert atmosphere affording without additive purification $\mathbf{L_{As,P}}$ as a white powder collected in 92 % yield. As for compound **B** based on the dppm ligand, a synthetic approach adapted of coordination driven supramolecular chemistry was conducted. The pre-assembled "U-shape" molecular clip $[Cu_2(\mu_2\text{-}(\mathbf{L_{As,P}})_2(CH_3CN)_4](PF_6)_2$ was formed *in situ* in a CH_2Cl_2 solution reacting two equivalents of $[Cu(CH_3CN)_4]PF_6$ with two equivalents of the $\mathbf{L_{As,P}}$ ligand. One equivalent of KCN was then added affording a clear colorless solution from which air stable single crystals of **A** were isolated by slow diffusion of pentane vapors through the crude mother solution, leading to a homogeneous batch of colorless polycrystalline powder in 89 % yield.[56] The RT $^{31}P\{^1H\}$ solution NMR spectrum of derivative **A** shows a singlet at -9.45 ppm (Fig. S1). This signal is deshielded compared to the non-coordinated $\mathbf{L_{As,P}}$ ligand (δ = -21.6 ppm, Fig. S1), suggesting that a coordination occurred with the Cu(I) ions. This chemical shift is consistent with the two broad singlets (δ = -8.5 ppm and -10.5 ppm) observed in the RT $^{31}P\{^1H\}$ spectrum of the metallacycle **B**, supporting a similar molecular structure.[32] The presence of PF_6^- counter-anions is confirmed by a septet at -144.4 ppm in the $^{31}P\{^1H\}$ spectrum (and by the typical $\upsilon(PF_6^-)$ vibrational band at 834 cm^{-1} in the infrared spectrum (Fig. S4). The RT ^1H solution NMR spectrum revealed the substitution of the acetonitrile ligands as no peak assigned to this fragment is detected (Fig. S1). This is in accordance with the solid-state infrared spectrum of the derivative **A** in which the typical signature of the υ(C≡N) stretching mode of the acetonitrile ligand[57] coordinated to a Cu(I) metal center at 2311 cm^{-1} is absent while a υ(C≡N) vibrational band at 2118 cm^{-1} characteristic of a Cu(I)–C≡N–Cu(I) fragment is observed (Fig. 1), at a similar energy than reported for the analogous metallacycle **B**.[32]

Crystal structure of the tetrametallic metallacycle A

The molecular structure of the derivative **A** was determined by single crystal X-ray diffraction study at 150 K.[56] The ORTEP diagram is represented in Fig. S10 and all the coordination sphere parameters are reported in Table S1-S3. A $[Cu_4(\mu_2\text{-}\mathbf{L_{As,P}})_4(CN)_2](PF_6)_2]$ assembly is revealed, having a tetrametallic scaffold similar to that of the compound **B** (Fig. 2). However, while derivative **B** crystallizes in the $P2_1/n$ space group of the monoclinic system,[32] the assembly **A** crystallizes in the P-1 space group of the triclinic crystal system (Table 1).

Table 1. Crystal data and structure refinement of compound **A**

CCDC number	2284699
Empirical formula	$C_{54}H_{50}As_2Cl_6Cu_2F_6NP_3$
Formula weight	1409.48
Temperature/K	150(2)
Crystal system	triclinic
Space group	P-1
a/Å	14.0932(16)
b/Å	14.5288(15)
c/Å	14.8566(15)
α/°	84.136(4)
β/°	74.702(4)
γ/°	73.177(4)
Volume/$Å^3$	2807.5(5)
Z	2
$\rho_{calc}g/cm^3$	1.667
μ/mm^{-1}	2.356
F(000)	1412.0
Crystal size/mm^3	0.450 × 0.380 × 0.340
Radiation	MoKα (λ = 0.71073)
2θ range for data collection/°	4.14 to 55.058
Index ranges	-18 ≤ h ≤ 18, -18 ≤ k ≤ 18, -18 ≤ l ≤ 19
Reflections collected	43687
Independent reflections	12827
Data/restraints/parameters	12827/213/705
Goodness-of-fit on F^2	1.099
Final R indexes [I>=2σ (I)]	R_1 = 0.0839, wR_2 = 0.2307
Final R indexes [all data]	R_1 = 0.0925, wR_2 = 0.2372
Largest diff. peak/hole / e $Å^{-3}$	3.37/-2.89

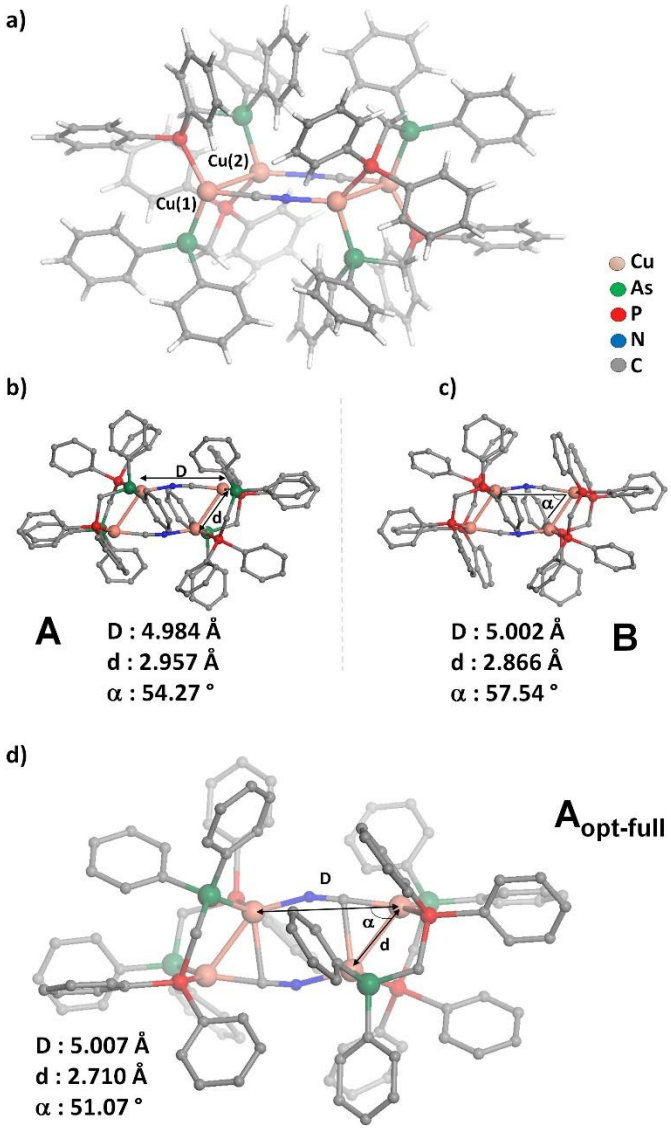

Fig. 2 a) View of the molecular X-ray structure of the derivative **A**; b) and c) Comparative views and selective metric parameters of the derivatives **A** and **B** respectively; d) view of the $\mathbf{A}_{\text{opt-full}}(S_0)$ calculated structure. (Counter-anions, H atoms (b), c) and d)) and solvent molecules have been omitted for clarity; location of the C and N atoms of the cyano ligands and of the P and As atoms of the $\mathbf{L}_{\mathbf{As,P}}$ ligands have been chosen arbitrarily).

The asymmetric unit observed in the single crystals of the derivative **A** contains one $[Cu_2(\mathbf{L}_{\mathbf{As,P}})_2CN]^+$ fragment, one PF_6^- counter-anion and three disordered CH_2Cl_2 solvent molecules. The derivative **A** is a tetrametallic metallacycle generated by the connection of two $[Cu_2(\mu_2\text{-}(\mathbf{L}_{\mathbf{As,P}})_2]^{2+}$ fragments by two cyanide ligands acting as ditopic linkers. The two Cu(I) ions of the $[Cu_2(\mu_2\text{-}(\mathbf{L}_{\mathbf{As,P}})_2]^{2+}$ fragment are crystallographically different and are denoted Cu(1) and Cu(2), Cu(1) being located at vertices of the acute angles of the metallacycle scaffold and Cu(2) at vertices of the obtuse ones. The four Cu(I) centers forming the metallacycle lie in the same plane. The carbon and nitrogen atoms of the cyanide bridging ligand are found to be disordered on two atomic positions for which equal occupancies were assigned. A similar treatment was applied for the arsenic and phosphorus atoms of the $\mathbf{L}_{\mathbf{As,P}}$ ligand since they are determined being equally distributed on both atomic positions corresponding to the donor atoms of the assembling $\mathbf{L}_{\mathbf{As,P}}$ ligands coordinated to the metal centers. Each Cu(I) ion is coordinated to two donor atoms (phosphorus and/or arsenic atoms) from two distinct $\mathbf{L}_{\mathbf{As,P}}$ ligands and to one CN^- ligand, resulting in a trigonal planar geometry characterized by six possible coordination sphere environments (P_2(N or C)$_1$, As_2(N or C)$_1$ or P_1As_1(N or C)$_1$). For the sake of simplicity in the description of the metric parameters of the inorganic metallacyclic '$Cu_4(CN)_2$' backbone of the assembly **A** and by analogy with the conclusions that were obtained from geometry optimization calculations based on DFT considering the possible arrangements of the carbon and nitrogen atoms of the cyano units in the molecular scaffold of the derivative **B**,[32] it will be considered that the nitrogen atoms of the cyano linkers are coordinated on the Cu(2) 'obtuse' metal center.

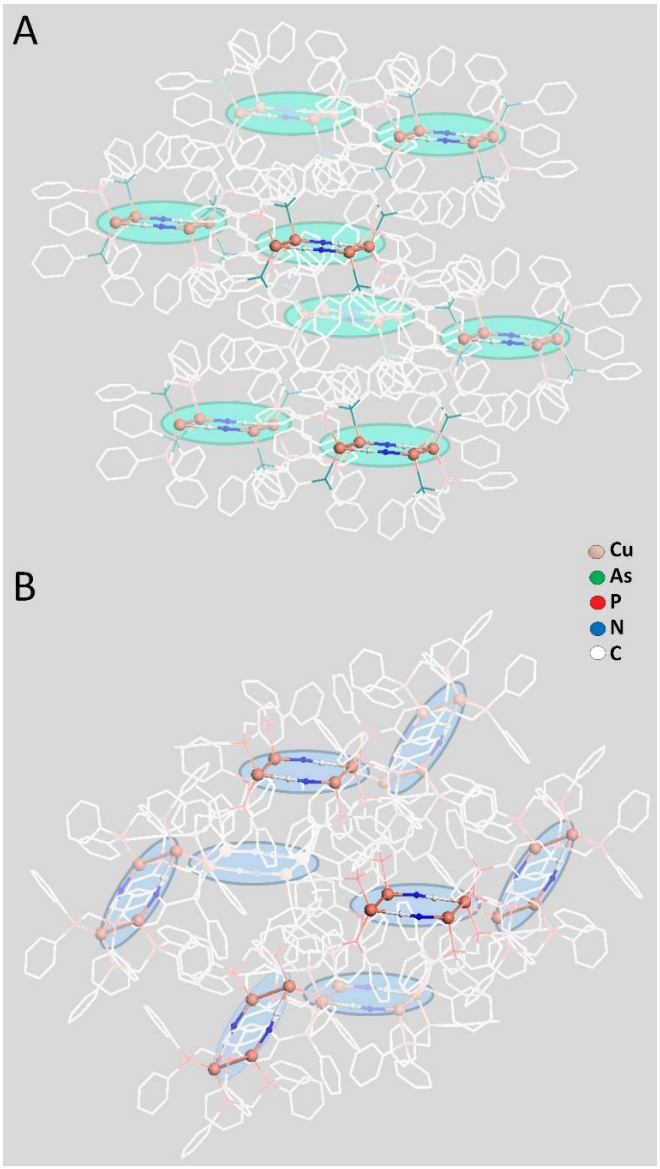

Fig. 3 Views of the extended stacking network observed in the single-crystals of **A** and **B** (the metalacyclic backbones are highlighted by colored ellipses, counter-anions, H atoms and solvent molecules have been omitted for clarity; carbon atoms (excepted the carbon atoms of the cyano ligands and pnictogen atoms are shown in line style).

The cyano linker are located within the plane of the metallacycle and have a slightly tilted coordination angle on the metal centers (Cu(1)–C≡N = 170.6(6)°; Cu(2)–N≡C = 173.5(3)°). Comparatively to the metallacycle **B** which exhibits short intermetallic distance ($d_{Cu\text{-}Cu}$ = 2.866(9) Å), the intermetallic distance Cu(I)···Cu(I) for compound **A** is slightly larger ($d_{Cu\text{-}Cu}$ = 2.957(1) Å), which is close to the upper limit of 2.9 Å generally considered for cuprophilic interactions. The PF_6^- anions are stabilized by hydrogen bonds with the phenyl rings of the $\mathbf{L}_{\mathbf{As,P}}$ ligand (d(F···H) = 2.515 – 2.642 Å).

Finally, in the solid-state crystal packing, metallacycles **A** share π-CH and π-π interactions with neighboring assemblies involving the phenyl rings of the $\mathbf{L_{As,P}}$ ligands. Moreover these discrete scaffolds are separated by the PF_6^- counter-anions and included CH_2Cl_2 molecules that occupy the cavities lying between the tetrametallic units **A**. In this triclinic P-1 packing, all metallacycles are orientated parallel (

Fig. 3). This is in a marked contrast with the monoclinic $P2_1/n$ packing observed in the crystals of the congener derivative **B** in which two markedly different orientations of the metallacycle are alternating (

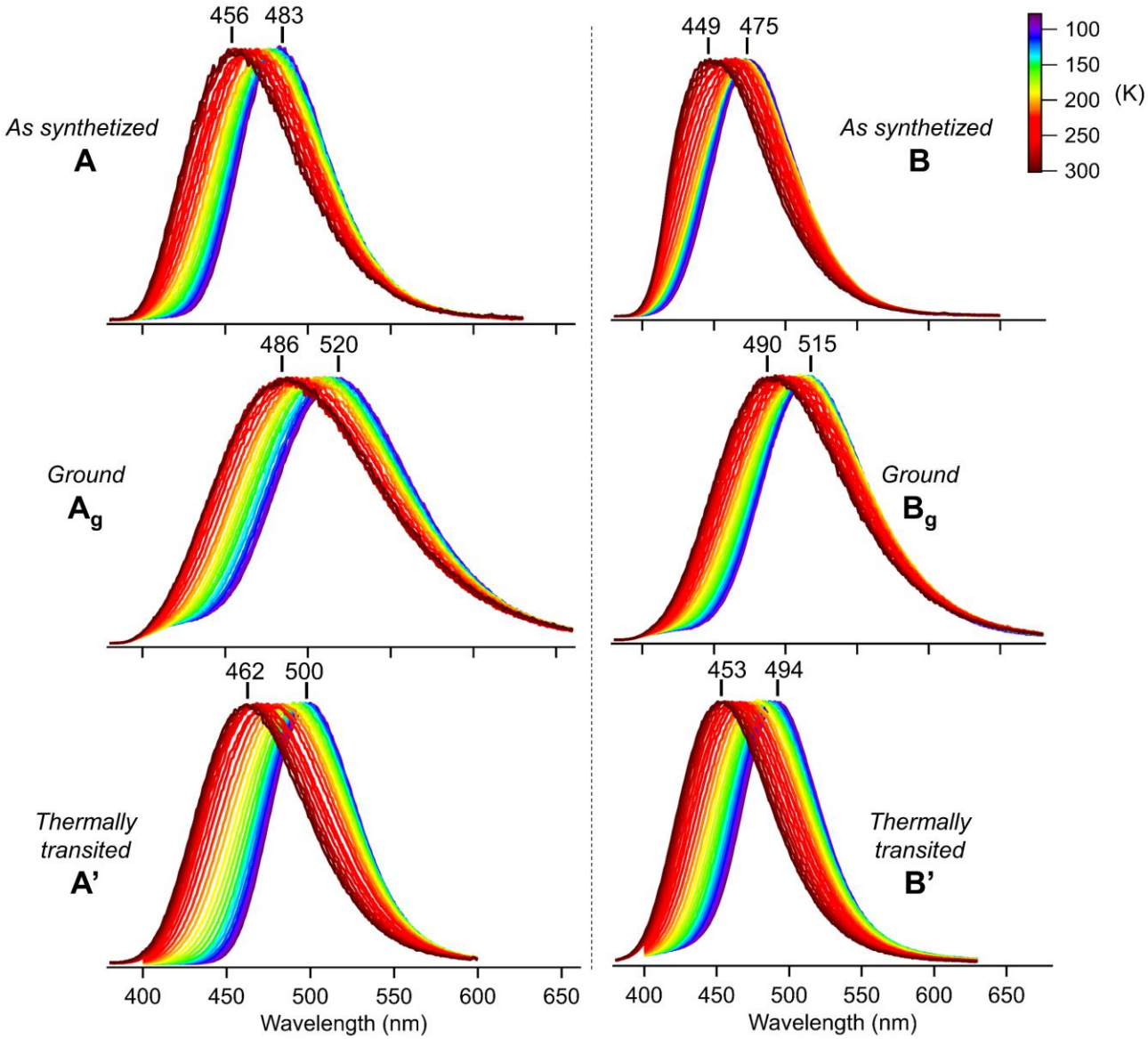

Fig. 3).

Photophysical properties

The RT solid-state absorption spectrum of derivative **A** shows a broad band in the UV region centered at 291 nm and a shoulder at 350 nm, typical of π–π* transition centered on the aromatic moieties of the $\mathbf{L_{As,P}}$ ligands (Fig. S13). The excitation spectrum at room temperature shows a large excitation domain from 300 nm to 365 nm with an intensity maximum centered at 356 nm (Fig. S15).

Fig. 4 Temperature dependent (80–300 K) normalized emission spectra of derivatives **A, A_g** and **A'** upon excitation at 356 nm, 372 nm and 365 nm, respectively, and of derivatives **B,**[32] **B_g** and **B'** upon excitation at 330 nm, 374 nm and 325 nm, respectively.

Upon excitation at 356 nm at 300 K, a polycrystalline batch of compound **A** exhibits a cyan eye-perceived solid-state luminescence (Fig. S12), characterized by a single broad unstructured emission band (FWHM = 3713 cm^{-1}, Fig. 4) centered at 456 nm together with biexponential decay times of τ_1 = 38 µs (58% relative rate) and τ_2 = 16 µs (42% relative rate) and an emission quantum yield (EQY) of 84 %. Upon cooling from 300 K to 80 K, the emission spectra of the molecular assembly **A** show a gradual and almost linear redshift ($\Delta\lambda_{em(300K\text{-}80K)}$ = 0.176 eV (1420 cm^{-1}), Fig. 4) associated with an increasing signal intensity (Fig. S16). At 80 K, an intense greenish eye-perceived emission is observed characterized by a large unstructured emission band (FWHM = 2344 cm^{-1}) centered at 483 nm, while the emission lifetimes τ_1(65%) and τ_2(35%) increases up to 224 µs and 111 µs, respectively. The temperature dependent shift of the solid-state emission spectra of **A** is completely reversible and the cyan luminescence observed at 300 K is recovered once the sample is warmed up. The detailed study of the temperature dependence of the excited state emission lifetime of **A** (Fig. S22) reveals biexponential radiative decay all along the temperature range from 300 K to 80 K. The thermal-variation profiles of τ_1 (long component) and τ_2 (short component) are reproducibly irregular. Likely, such a behavior can be assigned to the variety of the molecular conformations that can be generated due to the relative different localizations of the nitrogen and carbon atoms of the cyano ligands and/or of the phosphorus and the arsenic atoms of the $\mathbf{L_{As,P}}$ ligands in the tetrametallic metalacyclic backbone (affording six different possible coordination spheres for each metal center). For all of these possible conformers of compound **A**, different radiative relaxation emission processes probably coming from various excited emissive states (see quantum chemical calculation section) might be implied at each temperature. This renders tricky and questionable a fine assignment of the origin of the luminescence properties of compound **A**. However, all in all, the gross photophysical properties recorded for compound **A** probably emerge from an admixed between pure phosphorescence and TADF processes, this assumption being also supported by the TADF process highlighted as dominant radiative relaxation pathway in the case of the parent compound **B**.

Table 2. Photophysical data for species **A** (λ_{ex} = 356 nm), **A_g** (λ_{ex} = 372 nm), **A'** (λ_{ex} = 365 nm), **B**[57] (λ_{ex} = 330 nm), **B_g** (λ_{ex} = 374 nm) and **B'** (λ_{ex} = 325 nm) in the solid-state.

	d(Cu–Cu) (Å)	λ_{em} 300K (nm)	λ_{em} 80K (nm)	τ_{obs} 300K (µs)	τ_{obs} 80K (µs)	ϕ_{em} (%)	k_r (s^{-1})[a]	k_{nr} (s^{-1})[b]
A	2.957(1)	456	483	38 16	224 111	84	$2.2*10^4$	$4.2*10^3$
A_g	–	486	520	67 24 6	348 167 44	47	$7.0*10^3$	$7.9*10^3$
A'	–	462	500	45 12	328 262	82	–	–
B[32]	2.866(9)	449	475	40 10	200 40	72	$1.8*10^4$	$7.0*10^3$
B_g	–	490	515	66 26 7	439 238 80	74	$1.1*10^4$	$3.9*10^3$
B'	–	453	494	52	199	80	–	–

[a] $k_r = \phi_{em}/\tau_{obs}$; [b] $k_{nr} = (1-\phi_{em})/\tau_{obs}$; *Values for k_r and k_{nr} have been calculated considering the main component of RT τ_{obs}.*

The photophysical properties of the analogous compound **B** were previously published[32] and compare mostly to the ones characterized in this study for the derivative **A**. Indeed, metallacycle **B** shows a clear blue eye-perceived luminescence under excitation at 320 nm, centered at 449 nm at room temperature with biexponential decay times of 40 and 10 µs and an EQY of 72 % (Table 2). Upon cooling from 300 K to 80 K, a gradual redshift of the whole spectrum (Fig. 4) is also

observed affording an emission maximum at 475 nm, together with an increase of the biexponential decay times reaching 200 µs and 40 µs at 80 K. The temperature-dependent emission of the derivative **B** was assigned to a TADF mechanism. Such similarities highlighting only minor differences in the photophysics of derivatives **A** and **B** are quite puzzling, regarding previous results published in the literature, comparing phosphorus-based and arsenic-based related compounds that mostly reported different luminescence properties.[49–52] Regarding these unexpected results, theoretical molecular calculations were conducted to get insights into the influence of the substitution of one phosphorus atom by one arsenic atom on the molecular structures, the electronic properties and the photophysical properties of the derivatives **A** and **B**.

Quantum chemical calculations

Quantum chemical calculations have been performed employing DFT and time-dependent DFT (TD-DFT). The computational details are provided in the ESI. Full ($\mathbf{A_{opt\text{-}full}}(S_0)$, $\mathbf{B_{opt\text{-}full}}(S_0)$) and partially constrained ($\mathbf{A_{opt\text{-}const}}(S_0)$, $\mathbf{B_{opt\text{-}const}}(S_0)$) geometry optimizations in vacuum of compounds **A** and **B** in their ground state and full optimizations of their first singlet and triplet excited states (S_1, T_1) were performed (Tables S4-S6, Fig. S31). Electronic excitations (absorption properties; Table S7 and Fig. S32-S33) and excited states properties (emission; Table S8 and Fig. S34) were further simulated. Considering the possible conformers resulting from the different relative orientations of the cyano and the $\mathbf{L_{As,P}}$ ligands in the coordination spheres of the Cu(I) ions, the positioning of the carbon atoms *versus* the nitrogen atoms in the cyano units, and of the phosphorus and arsenic atoms in the $\mathbf{L_{As,P}}$ pnictogen ligands have been studied. The most stable arrangement corresponds to the configuration shown in the Fig. 2d with a centrosymmetric architecture having the nitrogen atoms of the cyano ligands coordinated on the Cu(I) obtuse metal center of the metalacyclic '$Cu_4(CN)_2$' backbone[32] and a phosphorus and an arsenic atom coordinated to each metal centers. This arrangement was kept for the rest of the computational study.

Regarding the $\mathbf{A_{opt\text{-}full}}(S_0)$ and $\mathbf{B_{opt\text{-}full}}(S_0)$ geometries, the gross metric data compare well with X-ray diffraction structures with deviations of less than 1.4 % on the bond distances. However, the metallacycle of the fully optimized structure $\mathbf{A_{opt\text{-}full}}(S_0)$ is not strictly planar with about 6° of deviation from planarity whereas the $\mathbf{B_{opt\text{-}full}}(S_0)$ metallacycle is quasi planar. Moreover, these fully-optimized geometries show shorter Cu···Cu distances than the X-ray structures (Table S5). These discrepancies strongly indicate that experimental metric data of the internal '$Cu_4(CN)_2$' metalacyclic backbones are influenced by the intermolecular environment. Indeed, previous investigations conducted on related luminescent 'Cu_6' and 'Cu_8Pd_1' assemblies have revealed that the crystal packing greatly influences the solid-state molecular conformations observed in single-crystals and therefore the metric data and the solid-state photophysical properties of these derivatives.[58,59] Taking these aspects into account, indirect simulations of these packing were performed by constraining the copper atomic positions in the metallacycles to those of the X-ray structures. These partially constrained geometry optimizations lead to $\mathbf{A_{opt\text{-}const}}(S_0)$ and $\mathbf{B_{opt\text{-}const}}(S_0)$. The main structural differences between the full and constrained geometries are observed within the metallacycle with an interaction only occurring in the fully optimized structures between one of the two copper atoms and the carbon atom of the neighboring cyano groups (Fig. 2d and S31). This leads to the shortening of the Cu···Cu distances of 0.24 Å and 0.19 Å respectively observed in $\mathbf{A_{opt\text{-}full}}(S_0)$ and $\mathbf{B_{opt\text{-}full}}(S_0)$ compared to the X-ray structural data.

Yet, these differences between the constrained and unconstrained geometries affect only moderately the electronic structures and the Franck Condon (FC) excited states in both systems (Table S7 and Fig. S32-S33). The lowest excited states T_1-FC and S_1-FC are MLCT character for both systems as it was already pointed out in the previous communication for **B**.[32] Interestingly, no major difference in the optical properties is calculated between **A** (mixed arsenic and phosphorus) and **B** (only phosphorus) systems. Spin-orbit coupling between S_1-FC and T_1-FC is moderate in all cases (6 to 10 cm^{-1}). Therefore, the substitutions of phosphorus by arsenic atoms do not lead to the strengthening of the calculated SOC values as it was initially anticipated.[49–53] The intersystem crossing is thus susceptible to be similar in both systems.

TD-DFT geometry relaxations of these excited states were performed. The most important structure features rely in all systems on the significant shortening of one or two Cu···Cu distances (Table S6) and the increased bending of Cu–cyano angles, leading to less symmetrical rectangular shape of the metalacyclic backbones. Interestingly enough, the Cu-pnictogen bonds are hardly affected upon relaxation after excitation. The main energies and characteristics of these fully optimized excited states are reported in Table S8. The SOC at the geometry of T_1 between T_1 and S_0 is slightly smaller than between S_1 and T_1, which leads to a long lifetime for T_1 if only spontaneous emission is considered (from 1 to 4 ms, Table S8). Considering that our calculations are done at 0 K and the level of theory used, the agreement between calculated phosphorescent and low temperature experimental emission wavelengths is satisfactory when considering the ground phases $\mathbf{A_g}$ and $\mathbf{B_g}$ luminescence properties (*vide supra*) as experimental solid-state phase references.

This set of calculated data reveals, in these Cu(I) polymetallic assemblies bearing pnictogen ligands, that the substitution of a phosphorus atom by an arsenic atom does not imply systematically an alteration of the SOC values. Indeed, if the electronic density lying on the pnictogen atoms is not implied in the electronic excitation processes, the impact of the substitution is inoperant. Importantly, in such situation, the intermolecular constraints applied on the gross metalacyclic backbone can induce subtle but noticeable structural alteration impacting optical changes, that may differentiate the photophysics of the assemblies regarding the pnictogen

atom present, in particular in the case of congener species bearing different crystal packing organizations.

Therefore, the emission properties of such assemblies are highly related with their molecular environment alteration, and can probe the application in the solid-state of diverse external stress offering potential access to attractive stimuli-sensitive luminescent molecular materials.

Stimuli-sensitive behavior

In a very general point of view, Cu(I) coordination complexes are endowed with labile and non-directional coordination spheres. This feature renders the gross conformation of Cu(I) species very sensitive to external stimuli and, concomitantly, photophysical properties can be impacted, affording potential new stimuli responsive multifunctional luminescent materials. Among the different classes of photochromic materials that exhibit promising potentials in versatile light emission related applications, a growing number of stimuli-responsive luminescent sensors is reported comprising rich thermo-, mechano-, vapo- or solvato-chromic luminescence properties. More specifically, mechanochromic luminescent derivatives constitute a class of chromogenic materials that can reversibly generate variation of their emission spectra in response to mechanical external stress, providing a direct visual detection of the environmental alteration. These optical variations primarily originate from force-induced transformations of molecular structure, disruption of structural arrangements and/or packing modes (molecular conformations and/or intermolecular interactions) in the solid-state. In the field of such mechanochromic molecular materials, most of the systems that have been reported are based on organic dyes[60–68], gold[69–79] or platinum[80–86] metal-complexes bearing rich variety of mechanochromic behaviors. Regarding the fascinating structural flexibility and luminescence properties that can be associated to Cu(I)-based molecular assemblies, these derivatives carry appealing potential for designing such stimuli-sensitive material,[1] and indeed attractive mechanochromic luminescent mononuclear or mainly polynuclear Cu(I) complexes have been reported in the recent years. [1,28,38,43,44,58]

The geometrical parameter differences between the crystal structures of the experimental derivative **A** and the optimized phase for the isolated species $\mathbf{A_{opt\text{-}full}}$ (in vacuum) (Fig. 2d) suggest that the crystal packing and the intermolecular interactions dictate the geometrical configuration adopted by this tetrametallic assembly in the solid-state crystalline structure, and concomitantly, the electronic structure, the relaxed geometries in the excited state and the photophysical properties. The influence of these intermolecular parameters in the photophysics of related Cu(I)-based stimuli-sensitive luminescent polymetallic assemblies were highlighted in related 'Cu_8Pd_1' assemblies[58] as a consequence of conformational changes involving non-covalent interaction alterations upon either grinding or melting of the bulk crystalline samples leading to emission properties modifications. Triggered by the TD-DFT calculations' conclusions that have highlighted such structural differences between the experimental and calculated ground state discrete structures (Fig. 2d), it can be anticipated that the photophysical processes lying in the **A** and **B** scaffolds should be impacted upon external constraints that could alter the crystal packing, affording new luminescent phases. This has motivated us to study the mechanochromic and thermolysis responses of solid-state polycrystalline samples of derivative **A**. Importantly, derivatives **A** and **B** crystallize in different space groups (respectively monoclinic and triclinic) in spite of their molecular structure similarities which will allow exploring the impact of the extended crystal structure organization differences on the stimuli-sensitive luminescence responses of such molecular solids.

Mechanical stress. Mechanical grinding of the polycrystalline powder of the derivatives **A** and **B** affords the colorless powder ground phases $\mathbf{A_g}$ and $\mathbf{B_g}$ (Fig. S12) that do not exhibit under visible light any eye-perceived change in the solid-state morphologies regarding the pristine phases. However, if this grinding is applied at RT under a UV-vis light irradiation of 365 nm, an instantaneous change of the eye-perceived cyan (**A**) or blue (**B**) light emitted is observed, affording eye-perceived greenish light emission at the places where the mechanical stress was applied. The infrared spectra of the phases $\mathbf{A_g}$ and $\mathbf{B_g}$ show a broadening and a shift to higher energy of the υ(C≡N) band reaching 2126 cm^{-1} and 2121 cm^{-1}, respectively (Fig. 1 and S4-S5). This reveals that structural alterations are generated in the metalacyclic backbones upon application of a mechanical stress, and might be attributed to metallacycle reorganizations leading to alternative conformers such as those observed in the theoretical study (interactions between the copper and the carbon atoms of the cyano bridging units in the geometry optimized ground state structures (Fig. 2d). The X-ray powder diffraction patterns conducted on the $\mathbf{A_g}$ and $\mathbf{B_g}$ phases, to get insights about the structural modifications potentially induced by the application of the mechanical stress on **A** and **B** derivatives, show two broad peaks around 7° and 20° revealing a major amorphization regarding the original crystalline **A** and **B** phases (Fig. 5 and S8). However, $^{31}P\{^1H\}$ and ^1H NMR spectra of the $\mathbf{A_g}$ and $\mathbf{B_g}$ phases dissolved in CD_2Cl_2 exhibit the same chemical shifts as derivatives **A** and **B**, respectively (Fig. S1 and S2). Moreover, the original crystalline phases of **A** and **B** are obtained after recrystallisation of $\mathbf{A_g}$ and $\mathbf{B_g}$ from pentane vapors diffusions in CH_2Cl_2 solutions (as confirmed by the crystals lattice parameters determination). Finally, the infrared spectra of these two recrystallized phases are identical with the initial spectra of phases **A** and **B** (Fig. S4 and S5). This set of measurements highlights that no chemical transformations are induced as a mechanical grinding is applied.

Solid-state absorption spectra at room temperature of derivatives $\mathbf{A_g}$ and $\mathbf{B_g}$ show a broad band in the UV region centered at 297 nm and 309 nm, respectively (Fig. S13 and S14) and their excitation spectrum shows two maxima at 318/372 nm ($\mathbf{A_g}$) and at 329/374 nm ($\mathbf{B_g}$) (Fig. S15). The room temperature solid-state emission spectrum of the phase $\mathbf{A_g}$ presents a large featureless band centered at 486 nm (Fig. 4

and S17, FWHM = 4833 cm^{-1}) upon excitation at 372 nm, which is significantly red-shifted ($\Delta\lambda_{em(\mathbf{Ag}\text{-}\mathbf{A})}$ = 0.168 eV (1345 cm^{-1})) compared to the emission spectrum of derivative **A**. Similarly, the room temperature solid-state emission spectrum of the phase $\mathbf{B_g}$ is characterized by a large featureless band with a maximum at 490 nm (λ_{ex} = 374 nm, FWHM = 4257 cm^{-1}), which has been red-shifted of $\Delta\lambda_{em(\mathbf{Bg}\text{-}\mathbf{B})}$ = 0.123 eV (991 cm^{-1}) compared to the emission of **B** (Fig. 4 and S20). For both phases $\mathbf{A_g}$ and $\mathbf{B_g}$, the emission lifetimes at 300 K were treated by a tri-exponential decay affording τ_1(24%) = 67 µs, τ_2(59%) = 24 µs, τ_3(17%) = 6 µs and τ_1(20%) = 66 µs, τ_2(65%) = 26 µs, τ_3(15%) = 7 µs, respectively while RT EQY reach 47 % ($\mathbf{A_g}$) and 74 % ($\mathbf{B_g}$). Upon cooling from 300 K to

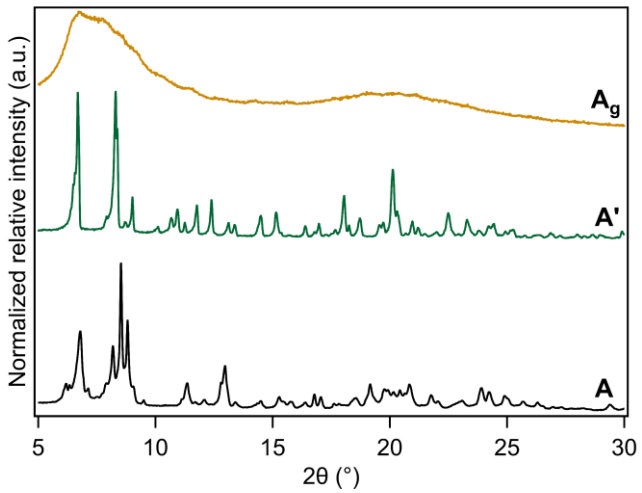

80 K, emission profiles of derivatives $\mathbf{A_g}$ and $\mathbf{B_g}$ exhibit a gradual red-shift reaching a green-yellow intense luminescence centered at 520 nm and 515 nm at 80 K respectively (compared to 483 nm for **A** and 475 nm for **B**), with emission lifetimes of 348 µs (τ_1(30%)), 167 µs (τ_2(63%) and 44 µs (τ_3(7%)) for $\mathbf{A_g}$ and 439 µs (τ_1(33%)), 238 µs (τ_2(60%)), 80 µs (τ_3(7%)) for $\mathbf{B_g}$. The temperature dependent shift of the solid-state emission spectra of these two phases is reversible and the greenish luminescence observed at 300 K is recovered once the samples are warmed up.

Fig. 5 PXRD patterns of derivatives **A**, $\mathbf{A_g}$, and **A'**.

This manual grinding applied on the crystalline solid-state batches of derivatives **A** and **B** induces therefore a major amorphization of the pristine phases and likely a local release of the non-covalent interaction networks formed between the metallacycles, generating multiple species bearing distinct emission properties.[87,88] However, the observed photophysical properties of the $\mathbf{A_g}$ and $\mathbf{B_g}$ phases (including the red-shift upon cooling of the single large band in the emission spectra and the general profile of the temperature dependance of the observed decay times of the excited states) support a preservation of the TADF relaxation processes evidenced in the pristine crystalline phases **A** and **B**.

Thermolysis. Thermal gravimetric analysis and differential thermal analysis (TGA-DTA) under nitrogen flux from RT to 950 °C reveal that compounds **A** and **B** decompose at 305 °C and 350 °C, respectively (Fig. S25 and S28). Beforehand, from 30 °C to 110 °C (**A**) and from 80 °C to 140 °C (**B**), a loss of mass of 3 and 4 %, respectively, takes place, together with endothermic peaks at 61 °C and 105°C (**A**) and at 126°C (**B**) that are tentatively assigned to the desorption of included guest solvent molecules and/or adsorbed molecular water (these derivatives are air-stable and were manipulated under ambient atmosphere). In addition, at 237 °C for **A** and 233 °C for **B**, an exothermic peak is observed, associated with no mass variation (Fig. S26 and 29), indicating that these thermal phenomena do not correspond to a decomposition process. Then, when heating the samples up to 270 °C and directly cooling down to RT, no thermal event is observed probing that an irreversible process occurred (Fig. S26 and 29). The solid-state infrared spectra of the new phases **A'** and **B'** present a single ν(C≡N) vibration observed at 2129 cm^{-1} and 2126 cm^{-1}, respectively (Fig. 1) shifted to higher frequencies compared to the values for the initial phases **A** and **B** (2118 cm^{-1}). Significant differences are also highlighted in the powder X-ray diffraction patterns of the phases **A'** and **B'** that show markedly different profiles compared to the native phases **A** and **B**, respectively (Fig. 5 and S8). These observations suggest that the exothermic peaks observed at 237 °C (**A'**) and 233 °C (**B'**) witness a crystalline phase transition associated with a conformational change of the molecular architecture of the tetrametallic metalacyclic backbone of the phases **A** and **B**, preserving the chemical structure of these derivatives, but impacting their spectroscopic signature, crystalline phases and also likely photophysical properties. This assumption is confirmed by the quantitative obtention of single crystals of native phases **A** and **B**, (evidenced by the determination of their unit cell parameters and infrared spectrum, Fig. S4-S5) from pentane vapor diffusions within CH_2Cl_2 solutions in which, respectively, the phases **A'** and **B'** were dissolved.

The two new phases, denoted **A'** and **B'**, are collected as polycrystalline white solids with an eye-perceived solid-state aspect very similar to the initial samples **A** and **B**. Under excitation at 365 nm and 325 nm, the transited solid phases **A'** and **B'** exhibit a clear-blue eye-perceived emission, characterized by a large band centered at 462 nm (FWHM = 2345 cm^{-1}) and 453 nm (FWHM = 3608 cm^{-1}), respectively, very reminiscent of the solid-state luminescence of **A** and **B** at room temperature (Fig. 4 and S18-S21). Yet, their excitation spectrum at RT is markedly different from the one of pristine phases **A** and **B**, showing two broad bands centered at 327 nm and 365 nm for **A'** and at 325 nm and 372 nm for **B'** (Fig. S15). In addition, the temperature dependent photophysical properties of **A'** and **B'** evidence slight but significant changes compared to **A** and **B**, such as a larger bathochromic shift in the emission spectra (Fig. 4) upon cooling from RT to 80 K, with $\Delta\lambda_{em(300\text{-}80K)}$ = 0.227 eV (1832 cm^{-1}) for **A'** and $\Delta\lambda_{em(300\text{-}80K)}$ = 0.204 eV (1645 cm^{-1}) for **B'**, while $\Delta\lambda_{em(300\text{-}80K)}$ = 0.176 eV (1420 cm^{-1}) for **A** and $\Delta\lambda_{em(300\text{-}80K)}$ = 0.151 eV (1219 cm^{-1}) for **B**. However, examination of the thermal variation of the decay time of the excited state reveals similar biexponential lifetime profiles for **A'** compared to **A**, for which τ_1(63%) and τ_2(37%) are equal to 45 µs and 12 µs at RT

and reaching 328 µs (33%) and 262 µs (67%) at 80 K (Table 2). The thermal variation of the decay time of the excited state recorded for **B'** is mono-exponential with values of 52 µs at 300 K and 199 µs at 80 K (Table 2). Finally, the values of the solid-state RT EQY for both phases **A'** and **B'** are *ca.* 80 % (Table 2). The temperature dependent shift of the solid-state emission spectra of these two phases is reversible and the eye-perceived blue-colored luminescence observed at 300 K is recovered once the samples are warmed up. Very likely, these data suggest that the radiative relaxation process assigned to TADF admixed with phosphorescence lying in the initial phases **A** and **B** are preserved but modulated in the thermally processed phases **A'** and **B'**.

Remarkably, these thermally transited phases **A'** and **B'** can also be formed by heating the amorphous ground phases $\mathbf{A_g}$ and $\mathbf{B_g}$ up to 230°C (see TGA-DTA curves, Fig. S27-S30). White solids whose PXRD diffractograms are similar to those of the phases **A'** and **B'** are obtained (Fig. S8-S9), demonstrating that upon solid-state thermolysis treatment of the amorphous $\mathbf{A_g}$ and $\mathbf{B_g}$ phases, the same crystalline states than obtained from the pristine **A** and **B** phases can be regenerated. This is confirmed by the IR spectrum of these phases that show the typical thinner and redshifted υ(C≡N) bands at 2129 cm^{-1} (**A'**) and 2126 cm^{-1} (**B'**) compared to $\mathbf{A_g}$ and $\mathbf{B_g}$, respectively (Fig. S6-S7).

Conclusions

With the preparation of the new metalacyclic assembly **A** based on the mixed arsenic-phosphorus $\mathbf{L_{As,P}}$ ligands, we demonstrated that the synthetic procedure applied to obtain the derivative **B** from the phosphorous dppm ligand can be extended to other ditopic pnictogen-based assembling ligands. While moderate intramolecular metric data alterations are determined in the discrete solid-state structure of the tetrametallic backbone of **A** compared to those of **B**, different extended crystalline packing are observed. Importantly, the luminescence properties of these two derivatives recorded on homogeneous polycrystalline powders are comparable, which is quite unexpected considering the generally admitted assumption that changing phosphorus atoms coordinated on the Cu(I) ions by arsenic atoms in similar molecular scaffolds should induce more efficient radiative relaxation processes as the SOC values would increase. TD-DFT calculations reveal that both **A** and **B** assemblies present very comparable electronic structures in which no electronic density lying on the pnictogen atoms is implied in the electronic excitation processes, explaining the neglectable impact of the substitution of the phosphorus centers by arsenic atoms on the recorded photophysical properties of **A** compared to **B**. Therefore, differences in the solid-state crystal structures may have in such systems an influence in the luminescence properties that can be competitive to those of the single atom SOC values. This questions in general the interpretation of the photophysical properties of such families of Cu(I) luminescent assemblies based on different organo-pnictogen ligands. A thorough analysis of both intramolecular metric data and intermetallic interaction networks must be conducted since antagonistic or complement effects may take place, in order to allow supplying an in-depth rationalization of the luminescence properties generated.

The stimuli-sensitivity of such photophysical properties toward intermolecular interaction alterations resulting of the application of external mechanical or thermal stress is also highlighted. This reveals that upon the preparation of a specific Cu(I) polymetallic assembly, various luminescent phases can be readily generated, whose photophysical parameters can greatly vary from a phase to another one (Fig. S24). Moreover, interconversion of all these species occurs reversibly, giving an access to a family of luminescent sensors from one pristine derivative. This set of results suggest that beside the molecular design of specific Cu(I)-based molecular assemblies bearing targeted luminescence properties, the consideration of the intermolecular interactions and extended packing can also lead to the preparation of manifold new luminescent species, including performant solid-state luminophores and stimuli-sensitive sensors.

Author Contributions

The manuscript was written through contributions of all authors. All authors have given approval to the final version of the manuscript.

Conflicts of interest

There are no conflicts to declare.

Acknowledgements

This work was supported by the CNRS, the ANR (ANR PRC SMAC and ANR PRCI SUPRALUM), the French 'Ministère de l'Enseignement Supérieur, de la Recherche et de l'Innovation' and the French 'Ministère des Affaires Etrangères' as well as by the Deutsche Forschungsgemeinschaft within the project Sche 384/42-1. C.L. thanks the Alexander von Humboldt Foundation for a fellowship for experienced researcher. R.U., K.C., and C.P. acknowledge support by the "Grand équipement national de calcul intensif (GENCI)" through HPC resources of CINES, TGCC and IDRIS (grants AD010800649R1).

Notes and references

1 S. Perruchas, Molecular copper iodide clusters: a distinguishing family of mechanochromic luminescent compounds, *Dalton Trans.*, 2021, **50**, 12031–12044.

2 V. W.-W. Yam, V. K.-M. Au and S. Y.-L. Leung, Light-Emitting Self-Assembled Materials Based on d^8 and d^{10} Transition Metal Complexes, *Chem. Rev.*, 2015, **115**, 7589–7728.

3 C. Bizzarri, E. Spuling, D. M. Knoll, D. Volz and S. Bräse, Sustainable metal complexes for organic light-emitting diodes (OLEDs), *Coord. Chem. Rev.*, 2018, **373**, 49–82.

4 I. O. Koshevoy, M. Krause and A. Klein, Non-covalent intramolecular interactions through ligand-design promoting

efficient photoluminescence from transition metal complexes, *Coord .Chem. Rev.*, 2020, **405**, 213094.
5 K. Tsuge, Y. Chishina, H. Hashiguchi, Y. Sasaki, M. Kato, S. Ishizaka and N. Kitamura, Luminescent copper(I) complexes with halogenido-bridged dimeric core, *Coord. Chem. Rev.*, 2016, **306**, 636–651.
6 A. Kobayashi and M. Kato, Stimuli-responsive Luminescent Copper(I) Complexes for Intelligent Emissive Devices, *Chem. Lett.*, 2017, **46**, 154–162.
7 H. Yersin, Ed., *Highly Efficient OLEDs: Materials Based on Thermally Activated Delayed Fluorescence*, Wiley, 1st edn., 2018.
8 R. Czerwieniec, M. J. Leitl, H. H. H. Homeier and H. Yersin, Cu(I) complexes – Thermally activated delayed fluorescence. Photophysical approach and material design, *Coord. Chem. Rev.*, 2016, **325**, 2–28.
9 C. Lescop, Coordination-Driven Syntheses of Compact Supramolecular Metallacycles toward Extended Metallo-organic Stacked Supramolecular Assemblies, *Acc. Chem. Res.*, 2017, **50**, 885–894.
10 C. Lescop, Coordination-Driven Supramolecular Synthesis Based on Bimetallic Cu(I) Precursors: Adaptive Behavior and Luminescence, *Chem. Rec.*, 2021, **21**, 544–557.
11 Y. Zhang, M. Schulz, M. Wächtler, M. Karnahl and B. Dietzek, Heteroleptic diimine–diphosphine Cu(I) complexes as an alternative towards noble-metal based photosensitizers: Design strategies, photophysical properties and perspective application, *Coord. Chem. Rev.*, 2018, **356**, 127–146.
12 A. Schlachter, K. Tanner and P. D. Harvey, Copper halide-chalcogenoether and -chalcogenone networks: Chain and cluster motifs, polymer dimensionality and photophysical properties, *Coord. Chem. Rev.*, 2021, **448**, 214176.
13 B. Hupp, C. Schiller, C. Lenczyk, M. Stanoppi, K. Edkins, A. Lorbach and A. Steffen, Synthesis, Structures, and Photophysical Properties of a Series of Rare Near-IR Emitting Copper(I) Complexes, *Inorg. Chem.*, 2017, **56**, 8996–9008.
14 G. Chakkaradhari, Y.-T. Chen, A. J. Karttunen, M. T. Dau, J. Jänis, S. P. Tunik, P.-T. Chou, M.-L. Ho and I. O. Koshevoy, Luminescent Triphosphine Cyanide d10 Metal Complexes, *Inorg. Chem.*, 2016, **55**, 2174–2184.
15 R. Hamze, J. L. Peltier, D. Sylvinson, M. Jung, J. Cardenas, R. Haiges, M. Soleilhavoup, R. Jazzar, P. I. Djurovich, G. Bertrand and M. E. Thompson, Eliminating nonradiative decay in Cu(I) emitters: >99% quantum efficiency and microsecond lifetime, *Science*, 2019, **363**, 601–606.
16 S. Shi, M. C. Jung, C. Coburn, A. Tadle, D. Sylvinson M. R., P. I. Djurovich, S. R. Forrest and M. E. Thompson, Highly Efficient Photo- and Electroluminescence from Two-Coordinate Cu(I) Complexes Featuring Nonconventional N-Heterocyclic Carbenes, *J. Am. Chem. Soc.*, 2019, **141**, 3576–3588.
17 A. S. Romanov, D. Di, L. Yang, J. Fernandez-Cestau, C. R. Becker, C. E. James, B. Zhu, M. Linnolahti, D. Credgington and M. Bochmann, Highly photoluminescent copper carbene complexes based on prompt rather than delayed fluorescence, *Chem. Commun.*, 2016, **52**, 6379–6382.
18 M. Mohankumar, F. Monti, M. Holler, F. Niess, B. Delavaux-Nicot, N. Armaroli, J.-P. Sauvage and J.-F. Nierengarten, Combining Topological and Steric Constraints for the Preparation of Heteroleptic Copper(I) Complexes, *Chem. Eur. J.*, 2014, **20**, 12083–12090.
19 M. J. Leitl, V. A. Krylova, P. I. Djurovich, M. E. Thompson and H. Yersin, Phosphorescence versus Thermally Activated Delayed Fluorescence. Controlling Singlet–Triplet Splitting in Brightly Emitting and Sublimable Cu(I) Compounds, *J. Am. Chem. Soc.*, 2014, **136**, 16032–16038.
20 S. Keller, A. Prescimone, H. Bolink, M. Sessolo, G. Longo, L. Martínez-Sarti, J. M. Junquera-Hernández, E. C. Constable, E. Ortí and C. E. Housecroft, Luminescent copper(I) complexes with bisphosphane and halogen-substituted 2,2′-bipyridine ligands, *Dalton Trans.*, 2018, **47**, 14263–14276.
21 S. Keller, M. Bantle, A. Prescimone, E. C. Constable and C. E. Housecroft, Hinged and Wide: A New P^P Ligand for Emissive [Cu(P^P)(N^N)][PF_6] Complexes, *Molecules*, 2019, **24**, 3934.
22 C. M. Brown, C. Li, V. Carta, W. Li, Z. Xu, P. H. F. Stroppa, I. D. W. Samuel, E. Zysman-Colman and M. O. Wolf, Influence of Sulfur Oxidation State and Substituents on Sulfur-Bridged Luminescent Copper(I) Complexes Showing Thermally Activated Delayed Fluorescence, *Inorg. Chem.*, 2019, **58**, 7156–7168.
23 J. Li, L. Wang, Z. Zhao, X. Li, X. Yu, P. Huo, Q. Jin, Z. Liu, Z. Bian and C. Huang, Two-Coordinate Copper(I)/NHC Complexes: Dual Emission Properties and Ultralong Room-Temperature Phosphorescence, *Angew. Chem. Int. Ed.*, 2020, **59**, 8210–8217.
24 M. Klein, N. Rau, M. Wende, J. Sundermeyer, G. Cheng, C.-M. Che, A. Schinabeck and H. Yersin, Cu(I) and Ag(I) Complexes with a New Type of Rigid Tridentate N,P,P-Ligand for Thermally Activated Delayed Fluorescence and OLEDs with High External Quantum Efficiency, *Chem. Mater.*, 2020, **32**, 10365–10382.
25 K. Xu, B.-L. Chen, F. Yang, L. Liu, X.-X. Zhong, L. Wang, X.-J. Zhu, F.-B. Li, W.-Y. Wong and H.-M. Qin, Largely Color-Tuning Prompt and Delayed Fluorescence: Dinuclear Cu(I) Halide Complexes with tert-Amines and Phosphines, *Inorg. Chem.*, 2021, **60**, 4841–4851.
26 J. Nitsch, F. Lacemon, A. Lorbach, A. Eichhorn, F. Cisnetti and A. Steffen, Cuprophilic interactions in highly luminescent dicopper(I)–NHC–picolyl complexes – fast phosphorescence or TADF?, *Chem. Commun.*, 2016, **52**, 2932–2935.
27 B. Huitorel, H. El Moll, R. Utrera-Melero, M. Cordier, A. Fargues, A. Garcia, F. Massuyeau, C. Martineau-Corcos, F. Fayon, A. Rakhmatullin, S. Kahlal, J.-Y. Saillard, T. Gacoin and S. Perruchas, Evaluation of Ligands Effect on the Photophysical Properties of Copper Iodide Clusters, *Inorg. Chem.*, 2018, **57**, 4328–4339.
28 A. Kobayashi, Y. Yoshida, M. Yoshida and M. Kato, Mechanochromic Switching between Delayed Fluorescence and Phosphorescence of Luminescent Coordination Polymers Composed of Dinuclear Copper(I) Iodide Rhombic Cores, *Chem. Eur. J.*, 2018, **24**, 14750–14759.
29 A. V. Artem'ev, E. A. Pritchina, M. I. Rakhmanova, N. P. Gritsan, I. Yu. Bagryanskaya, S. F. Malysheva and N. A. Belogorlova, Alkyl-dependent self-assembly of the first red-emitting zwitterionic {Cu_4I_6} clusters from [alkyl-P(2-Py)$_3$]+ salts and CuI: when size matters, *Dalton Trans.*, 2019, **48**, 2328–2337.
30 A. Yu. Baranov, A. S. Berezin, D. G. Samsonenko, A. S. Mazur, P. M. Tolstoy, V. F. Plyusnin, I. E. Kolesnikov and A. V. Artem'ev, New Cu(i) halide complexes showing TADF combined with room temperature phosphorescence: the balance tuned by halogens, *Dalton Trans.*, 2020, **49**, 3155–3163.
31 A. Kobayashi, R. Arata, T. Ogawa, M. Yoshida and M. Kato, Effect of Water Coordination on Luminescent Properties of Pyrazine-Bridged Dinuclear Cu(I) Complexes, *Inorg. Chem.*, 2017, **56**, 4280–4288.
32 M. El Sayed Moussa, S. Evariste, H.-L. Wong, L. Le Bras, C. Roiland, L. Le Polles, B. Le Guennic, K. Costuas, V. W.-W. Yam and C. Lescop, A solid state highly emissive Cu(I) metallacycle:

promotion of cuprophilic interactions at the excited states, *Chem. Commun.*, 2016, **52**, 11370–11373.

33 S. Bassoli, G. Attilio Ardizzoia, B. Therrien and S. Brenna, Phosphorescence enhancement by close metal–metal interaction in T1 excited state in a dinuclear copper(I) complex, *Dalton Trans.*, 2019, **48**, 9276–9283.

34 F. Moutier, J. Schiller, G. Calvez and C. Lescop, Self-assembled luminescent Cu(I) tetranuclear metallacycles based on 3,3'-bipyridine ligands, *Org. Chem. Front.*, 2021, **8**, 2893–2902.

35 S. Chen, J. Gao, J. Chang, Y. Li, C. Huangfu, H. Meng, Y. Wang, G. Xia and L. Feng, Family of Highly Luminescent Pure Ionic Copper(I) Bromide Based Hybrid Materials, *ACS Appl. Mater. Interfaces*, 2019, **11**, 17513–17520.

36 C. Sun, L. Llanos, P. Arce, A. Oliver, R. Wannemacher, J. Cabanillas-Gonzalez, L. Lemus and D. Aravena, Nuclearity Control for Efficient Thermally Activated Delayed Fluorescence in a Cu^{I} Complex and its Halogen-Bridged Dimer, *Chem. Mater.*, 2021, **33**, 6383–6393.

37 T. Hasegawa, A. Kobayashi, H. Ohara, M. Yoshida and M. Kato, Emission Tuning of Luminescent Copper(I) Complexes by Vapor-Induced Ligand Exchange Reactions, *Inorg. Chem.*, 2017, **56**, 4928–4936.

38 B. Hupp, J. Nitsch, T. Schmitt, R. Bertermann, K. Edkins, F. Hirsch, I. Fischer, M. Auth, A. Sperlich and A. Steffen, Stimulus-Triggered Formation of an Anion–Cation Exciplex in Copper(I) Complexes as a Mechanism for Mechanochromic Phosphorescence, *Angew. Chem. Int. Ed.*, 2018, **57**, 13671–13675.

39 C. Li, W. Li, A. F. Henwood, D. Hall, D. B. Cordes, A. M. Z. Slawin, V. Lemaur, Y. Olivier, I. D. W. Samuel and E. Zysman-Colman, Luminescent Dinuclear Copper(I) Complexes Bearing an Imidazolylpyrimidine Bridging Ligand, *Inorg. Chem.*, 2020, **59**, 14772–14784.

40 T. Hayashi, A. Kobayashi, H. Ohara, M. Yoshida, T. Matsumoto, H.-C. Chang and M. Kato, Vapochromic Luminescence and Flexibility Control of Porous Coordination Polymers by Substitution of Luminescent Multinuclear Cu(I) Cluster Nodes, *Inorg. Chem.*, 2015, **54**, 8905–8913.

41 Q. Benito, C. M. Balogh, H. El Moll, T. Gacoin, M. Cordier, A. Rakhmatullin, C. Latouche, C. Martineau-Corcos and S. Perruchas, Luminescence Vapochromism of a Dynamic Copper Iodide Mesocate, *Chem. Eur. J.*, 2018, **24**, 18868–18872.

42 Z.-C. Shi, W. Chen, S.-Z. Zhan, M. Li, M. Xie, Y. Y. Li, S. W. Ng, Y.-L. Huang, Z. Zhang, G.-H. Ning and D. Li, Guest effects on crystal structure and phosphorescence of a Cu_6L_3 prismatic cage, *Inorg. Chem. Front.*, 2020, **7**, 1437–1444.

43 S. Perruchas, X. F. Le Goff, S. Maron, I. Maurin, F. Guillen, A. Garcia, T. Gacoin and J.-P. Boilot, Mechanochromic and Thermochromic Luminescence of a Copper Iodide Cluster, *J. Am. Chem. Soc.*, 2010, **132**, 10967–10969.

44 Q. Benito, X. F. Le Goff, S. Maron, A. Fargues, A. Garcia, C. Martineau, F. Taulelle, S. Kahlal, T. Gacoin, J.-P. Boilot and S. Perruchas, Polymorphic Copper Iodide Clusters: Insights into the Mechanochromic Luminescence Properties, *J. Am. Chem. Soc.*, 2014, **136**, 11311–11320.

45 S. Evariste, A. M. Khalil, S. Kerneis, C. Xu, G. Calvez, K. Costuas and C. Lescop, Luminescent vapochromic single crystal to single crystal transition in one-dimensional coordination polymer featuring the first Cu(I) dimer bridged by an aqua ligand, *Inorg. Chem. Front.*, 2020, **7**, 3402–3411.

46 S. Ogawa, H. Katsuragi, T. Ikeda, K. Oshima, S. Satokawa, Y. Yamazaki and T. Tsubomura, Dual mechanoluminescence system comprising a solid-state di-copper(I) complex containing N-heterocyclic carbene ligands, *Dalton Trans.*, 2021, **50**, 8845–8850.

47 N. V. S. Harisomayajula, S. Makovetskyi and Y.-C. Tsai, Cuprophilic Interactions in and between Molecular Entities, *Chem. Eur. J.*, 2019, **25**, 8936–8954.

48 H. Yersin, R. Czerwieniec, U. Monkowius, R. Ramazanov, R. Valiev, M. Z. Shafikov, W.-M. Kwok and C. Ma, Intersystem crossing, phosphorescence, and spin-orbit coupling. Two contrasting Cu(I)-TADF dimers investigated by milli- to micro-second phosphorescence, femto-second fluorescence, and theoretical calculations, *Coord. Chem. Rev.*, 2023, **478**, 214975.

49 A. V. Artem'ev, Y. V. Demyanov, M. I. Rakhmanova and I. Yu. Bagryanskaya, Pyridylarsine-based Cu(I) complexes showing TADF mixed with fast phosphorescence: a speeding-up emission rate using arsine ligands, *Dalton Trans.*, 2022, **51**, 1048–1055.

50 R. Kobayashi, H. Imoto and K. Naka, Stimuli-Responsive Emission of Dinuclear Rhombic Copper(I) Iodide Complexes Having Triphenylarsine and N-Heteroaromatic Co-Ligands, *Eur. J. Inorg. Chem.*, 2020, **2020**, 3548–3553.

51 R. Kobayashi, T. Yumura, H. Imoto and K. Naka, Homo- and hetero-metallophilicity-driven synthesis of highly emissive and stimuli-responsive Au(I)–Cu(I) double salts, *Chem. Commun.*, 2021, **57**, 5382–5385.

52 M. F. Galimova, E. M. Zueva, A. B. Dobrynin, I. E. Kolesnikov, R. R. Musin, E. I. Musina and A. A. Karasik, Luminescent Cu_4I_4-cubane clusters based on N-methyl-5,10-dihydrophenarsazines, *Dalton Trans.*, 2021, **50**, 13421–13429.

53 M. F. Galimova, E. M. Zueva, A. B. Dobrynin, A. I. Samigullina, R. R. Musin, E. I. Musina and A. A. Karasik, Cu_4I_4-cubane clusters based on 10-(aryl)phenoxarsines and their luminescence, *Dalton Trans.*, 2020, **49**, 482–491.

54 M. Montalti, A. Credi, L. Prodi, M. T. Gandolfi, J. Michl and V. Balzani, *Handbook of photochemistry*, CRC/Taylor & Francis, Boca Raton, Third edition., 2020.

55 J. W. Dube, Y. Zheng, W. Thiel and M. Alcarazo, α-Cationic Arsines: Synthesis, Structure, Reactivity, and Applications, *J. Am. Chem. Soc.*, 2016, **138**, 6869–6877.

56 For experimental details, spectroscopic, X-ray diffraction data and computational studies views see ESI

57 I. S. Kritchenkov, J. R. Shakirova and S. P. Tunik, Efficient one-pot green synthesis of tetrakis(acetonitrile)copper(i) complex in aqueous media, *RSC Adv.*, 2019, **9**, 15531–15535.

58 F. Moutier, J. Schiller, C. Lecourt, A. M. Khalil, V. Delmas, G. Calvez, K. Costuas and C. Lescop, Impact of Intermolecular Non-Covalent Interactions in a $Cu^{I}_{8}Pd^{II}_{1}$ Discrete Assembly: Conformers' Geometries and Stimuli-Sensitive Luminescence Properties, *Chem. Eur. J.*, 2022, **28**, e202104497.

59 M. E. S. Moussa, A. M. Khalil, S. Evariste, H.-L. Wong, V. Delmas, B. L. Guennic, G. Calvez, K. Costuas, V. W.-W. Yam and C. Lescop, ntramolecular rearrangements guided by adaptive coordination-driven reactions toward highly luminescent polynuclear Cu(I) assemblies, *Inorg. Chem. Front.*, 2020, **7**, 1334–1344.

60 S. Ito, Recent Advances in Mechanochromic Luminescence of Organic Crystalline Compounds, *Chem. Lett.*, 2021, **50**, 649–660.

61 L. Huang, C. Qian and Z. Ma, Stimuli-Responsive Purely Organic Room-Temperature Phosphorescence Materials, *Chem. Eur. J.*, 2020, **26**, 11914–11930.

62 M. Yang, I. S. Park, Y. Miyashita, K. Tanaka and T. Yasuda Mechanochromic Delayed Fluorescence Switching in Propeller-Shaped Carbazole–Isophthalonitrile Luminogens with Stimuli-

Responsive Intramolecular Charge-Transfer Excited States,, *Angew. Chem. Int. Ed.*, 2020, **132**, 14059–14065.
63 S. Nagai, M. Yamashita, T. Tachikawa, T. Ubukata, M. Asami and S. Ito, Efficient and versatile mechanochromic luminescence of phenanthroimidazolylbenzothiadiazoles: tricolor switching and directional control over the chromism, *J. Mater. Chem. C*, 2019, **7**, 4988–4998.
64 S.-N. Lei, H. Xiao, Y. Zeng, C.-H. Tung, L.-Z. Wu and H. Cong, BowtieArene: A Dual Macrocycle Exhibiting Stimuli-Responsive Fluorescence, *Angew. Chem. Int. Ed.*, 2020, **59**, 10059–10065.
65 K. Isayama, N. Aizawa, J. Y. Kim and T. Yasuda, Modulating Photo- and Electroluminescence in a Stimuli-Responsive π-Conjugated Donor–Acceptor Molecular System, *Angew. Chem. Int. Ed.*, 2018, **130**, 12158–12162.
66 J. Guan, F. Xu, C. Tian, L. Pu, M.-S. Yuan and J. Wang, Tricolor Luminescence Switching by Thermal and Mechanical Stimuli in the Crystal Polymorphs of Pyridyl-substituted Fluorene, *Chem. Asian J.*, 2019, **14**, 216–222.
67 H. Tsujimoto, D.-G. Ha, G. Markopoulos, H. S. Chae, M. A. Baldo and T. M. Swager, Thermally Activated Delayed Fluorescence and Aggregation Induced Emission with Through-Space Charge Transfer, *J. Am. Chem. Soc.*, 2017, **139**, 4894–4900.
68 Z. Yang, Z. Chi, Z. Mao, Y. Zhang, S. Liu, J. Zhao, M. P. Aldred and Z. Chi, Recent advances in mechano-responsive luminescence of tetraphenylethylene derivatives with aggregation-induced emission properties, *Mat. Chem. Front.*, 2018, **2**, 861–890.
69 H. Ito, M. Muromoto, S. Kurenuma, S. Ishizaka, N. Kitamura, H. Sato and T. Seki, Mechanical stimulation and solid seeding trigger single-crystal-to-single-crystal molecular domino transformations, *Nat Commun*, 2013, **4**, 2009.
70 J. Schneider, Y.-A. Lee, J. Pérez, W. W. Brennessel, C. Flaschenriem and R. Eisenberg, Strong Intra- and Intermolecular Aurophilic Interactions in a New Series of Brilliantly Luminescent Dinuclear Cationic and Neutral Au(I) Benzimidazolethiolate Complexes, *Inorg. Chem.*, 2008, **47**, 957–968.
71 A. Laguna, T. Lasanta, J. M. López-de-Luzuriaga, M. Monge, P. Naumov and M. E. Olmos, Combining Aurophilic Interactions and Halogen Bonding To Control the Luminescence from Bimetallic Gold−Silver Clusters, *J. Am. Chem. Soc.*, 2010, **132**, 456–457.
72 M. Osawa, I. Kawata, S. Igawa, M. Hoshino, T. Fukunaga and D. Hashizume, Vapochromic and Mechanochromic Tetrahedral Gold(I) Complexes Based on the 1,2-Bis(diphenylphosphino)benzene Ligand, *Chem. Eur. J.*, 2010, **16**, 12114–12126.
73 I. O. Koshevoy, C.-L. Lin, A. J. Karttunen, M. Haukka, C.-W. Shih, P.-T. Chou, S. P. Tunik and T. A. Pakkanen, Octanuclear gold(i) alkynyl-diphosphine clusters showing thermochromic luminescence, *Chem. Commun.*, 2011, **47**, 5533–5535.
74 A. Deák, C. Jobbágy, G. Marsi, M. Molnár, Z. Szakács and P. Baranyai, Anion-, Solvent-, Temperature-, and Mechano-Responsive Photoluminescence in Gold(I) Diphosphine-Based Dimers, *Chem. Eur. J.*, 2015, **21**, 11495–11508.
75 Z. Chen, J. Liang, Y. Nie, X. Xu, G.-A. Yu, J. Yin and S. Hua Liu, *Dalton Trans.*, A novel carbazole-based gold(i) complex with interesting solid-state, multistimuli-responsive characteristics, 2015, **44**, 17473–17477.
76 T. Seki, K. Kobayashi, T. Mashimo and H. Ito, A gold isocyanide complex with a pendant carboxy group: orthogonal molecular arrangements and hypsochromically shifted luminescent mechanochromism, *Chem. Commun.*, 2018, **54**, 11136–11139.
77 F. C.-M. Leung, S. Y.-L. Leung, C. Y.-S. Chung and V. W.-W. Yam, Metal–Metal and π–π Interactions Directed End-to-End Assembly of Gold Nanorods, *J. Am. Chem. Soc.*, 2016, **138**, 2989–2992.
78 N. M.-W. Wu, M. Ng and V. W.-W. Yam, Photochromic Benzo[b]phosphole Alkynylgold(I) Complexes with Mechanochromic Property to Serve as Multistimuli-Responsive Materials, *Angew. Chem. Int. Ed.*, 2019, **58**, 3027–3031.
79 T. Seki, K. Ida, H. Sato, S. Aono, S. Sakaki and H. Ito, Aurophilicity-Mediated Construction of Emissive Porous Molecular Crystals as Versatile Hosts for Liquid and Solid Guests, *Chem. Eur. J.*, 2020, **26**, 735–744.
80 Y. Nishiuchi, A. Takayama, T. Suzuki and K. Shinozaki, A Polymorphic Platinum(II) Complex: Yellow, Red, and Green Polymorphs and X-ray Crystallography of [Pt(fdpb)Cl] [Hfdpb = 1,3-Bis(5-trifluoromethyl-2-pyridyl)benzene], *Eur. J. Inorg. Chem.* 2011, **2011**, 1815–1823.
81 S. J. Choi, J. Kuwabara, Y. Nishimura, T. Arai and T. Kanbara, Two-step Changes in Luminescence Color of Pt(II) Complex Bearing an Amide Moiety by Mechano- and Vapochromism, *Chem. Lett.*, 2012, **41**, 65–67.
82 X. Zhang, J.-Y. Wang, J. Ni, L.-Y. Zhang and Z.-N. Chen, Vapochromic and Mechanochromic Phosphorescence Materials Based on a Platinum(II) Complex with 4-Trifluoromethylphenylacetylide, *Inorg. Chem.*, 2012, **51**, 5569–5579.
83 A. Han, P. Du, Z. Sun, H. Wu, H. Jia, R. Zhang, Z. Liang, R. Cao and R. Eisenberg, Reversible Mechanochromic Luminescence at Room Temperature in Cationic Platinum(II) Terpyridyl Complexes, *Inorg. Chem.*, 2014, **53**, 3338–3344.
84 A. Chowdhury, P. Howlader and P. S. Mukherjee, Mechano-fluorochromic Pt^{II} Luminogen and Its Cysteine Recognition, *Chem. Eur. J.*, 2016, **22**, 1424–1434.
85 C. Cuerva, J. A. Campo, M. Cano and C. Lodeiro Multi-Stimuli-Responsive Properties of Aggregation-Enhanced Emission-Active Unsymmetrical Pt^{II} Metallomesogens through Self-Assembly,, *Chem. Eur. J.*, 2019, **25**, 12046–12051.
86 X. Zhang, L.-Y. Zhang, J.-Y. Wang, F.-R. Dai and Z.-N. Chen, Two-step phosphorescent mechanochromism due to intramolecular deformation, *J. Mater. Chem. C*, 2020, **8**, 715–720.
87 R. Utrera-Melero, B. Huitorel, M. Cordier, F. Massuyeau, J.-Y. Mevellec, N. Stephant, P. Deniard, C. Latouche, C. Martineau-Corcos and S. Perruchas, Mechanically responsive luminescent films based on copper iodide clusters, *J. Mater. Chem. C*, 2021, **9**, 7991–8001.
88 B. Huitorel, R. Utrera-Melero, F. Massuyeau, J.-Y. Mevelec, B. Baptiste, A. Polian, T. Gacoin, C. Martineau-Corcos and S. Perruchas, Luminescence mechanochromism of copper iodide clusters: a rational investigation, *Dalton Trans.*, 2019, **48**, 7899–7909.